



Dalton  
Transactions

**Highly covalent metal-ligand  $\pi$  bonding in chelated bis- and tris(iminoxolene) complexes of osmium and ruthenium**

Journal:	<i>Dalton Transactions</i>
Manuscript ID	DT-ART-04-2020-001287.R1
Article Type:	Paper
Date Submitted by the Author:	28-Apr-2020
Complete List of Authors:	Gianino, Jacqueline; University of Notre Dame, Department of Chemistry and Biochemistry Brown, Seth; University of Notre Dame, Department of Chemistry and Biochemistry

SCHOLARONE™  
Manuscripts



## Highly covalent metal-ligand $\pi$ bonding in chelated bis- and tris(iminoxolene) complexes of osmium and ruthenium

Jacqueline Gianino and Seth N. Brown\*<sup>a</sup>

Received 00th January 20xx,  
Accepted 00th January 20xx

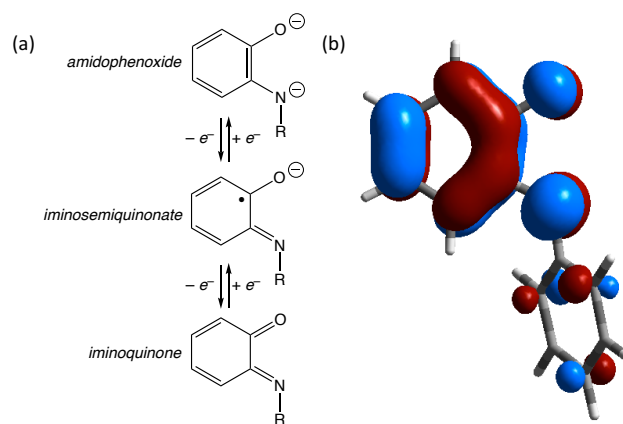
DOI: 10.1039/x0xx00000x

www.rsc.org/

The bis(aminophenol) 2,2'-biphenylbis(3,5-di-*tert*-butyl-2-hydroxyphenylamine) (ClipH<sub>4</sub>) forms *trans*-(Clip)Os(py)<sub>2</sub> upon aerobic reaction of the ligand with {(*p*-cymene)OsCl<sub>2</sub>)}<sub>2</sub> in the presence of pyridine and triethylamine. A more oxidized species, *cis*- $\beta$ -(Clip)Os(OCH<sub>2</sub>CH<sub>2</sub>O), is formed from reaction of the ligand with the osmium(VI) complex OsO(OCH<sub>2</sub>CH<sub>2</sub>O)<sub>2</sub>, and reacts with Me<sub>3</sub>SiCl to give the chloro complex *cis*- $\beta$ -(Clip)OsCl<sub>2</sub>. Octahedral osmium and ruthenium tris-iminoxolene complexes are formed from the chelating ligand tris(2-(3',5'-di-*tert*-butyl-2'-hydroxyphenyl)amino-4-methylphenyl)amine (MeClampH<sub>6</sub>) on aerobic reaction with divalent metal precursors. The complexes' structural and electronic features are well described using a simple bonding model that emphasizes the covalency of the  $\pi$  bonding between the metal and iminoxolene ligands rather than attempting to dissect the parts into discrete oxidation states. Emphasizing the continuity of bonding between disparate complexes, the structural data from a variety of Os and Ru complexes show good correlations to  $\pi$  bond order, and the response of the intraligand bond distances to the bond order can be analyzed to illuminate the polarity of the bonding between metal and the redox-active orbital on the iminoxolene. The osmium compounds'  $\pi$  bonding orbitals are about 40% metal-centered and 60% ligand-centered, with the ruthenium compounds' orbitals about 65% metal-centered and 35% ligand-centered.

### Introduction

Iminoxolenes are prototypical examples of redox-active ligands, capable of displaying oxidation states ranging from the fully reduced amidophenoxide to the radical anion iminosemiquinonate to the neutral iminoquinone (Scheme 1a). The stability of these oxidation states arises because the in-phase combination of heteroatom lone pair orbitals is  $\pi$ -antibonding with respect to a filled  $\pi$  orbital of the benzene ring (Scheme 1b). This redox-active orbital (RAO) is thus of a moderate energy and can readily accept or lose electrons. Since these ligands can potentially adopt multiple oxidation states, the literature of iminoxolene complexes, as well as that of the isoelectronic dioxolene complexes,<sup>1</sup> is dominated by attempts to assign discrete oxidation states to the ligands and to the metal. This bonding description, as in all oxidation state descriptions, is physically correct only in the limit of strictly ionic bonding, where electrons must be either on the ligand or on the metal, but cannot be shared between them. For dioxolene and iminoxolene complexes, this model has generally worked well for first-row metals and for complexes of the early and late transition metals. In these cases, the



Scheme 1 (a) Oxidation states and (b) Redox-active orbital (RAO) of iminoxolene ligands.

bonding is indeed substantially ionic in nature. For the first-row metals, the modest orbital overlap and, for the later metals, the propensity to form high-spin complexes with correspondingly long metal-ligand bonds, lead to little covalency in the metal-ligand bonds. With early transition metals, the metal *d* orbitals are higher in energy than the RAO. The metals are generally found in their highest oxidation state, and any redox changes are localized on the ligand.<sup>2</sup> Conversely, late transition metals have much lower-lying *d* $\pi$  orbitals which are invariably filled, again with the consequence that redox changes are localized on the ligands.<sup>3</sup> In all these

<sup>a</sup> Department of Chemistry and Biochemistry, 251 Nieuwland Science Hall, University of Notre Dame, Notre Dame, IN 46556-5670, USA. Fax: 01 574 631 6652; Tel: 01 574 631 4659; E-mail: Seth.N.Brown.114@nd.edu

Electronic Supplementary Information (ESI) available: Spin density plot of [(Clip)Os(py)<sub>2</sub>]<sup>+</sup>, literature MOS data, and computational details. CCDC 1994511-1994514. See DOI: 10.1039/x0xx00000x

compounds, electron delocalization between metal and ligand is minimal, and it is sensible to speak of a "physical" oxidation state.<sup>4</sup>

But the 4*d* and 5*d* metals in the middle of the periodic table are expected to have substantial covalency in their metal-iminoxolene  $\pi$  bonding, due to the similar orbital energy of the metals to the ligand RAO. Evidence of this covalency is apparent even as far to the left as molybdenum, whose iminoxolene complexes form very strong  $\pi$  bonds<sup>5</sup> that significantly perturb the structures of the coordinated amidophenoxide ligand.<sup>6</sup> The structural changes are reminiscent of those seen on ligand oxidation, but correspond to noninteger apparent oxidation states.<sup>7</sup> They are thus more consistent with redistribution of electron density due to (polar) covalent bonding rather than outright electron transfer.

Covalency is expected to peak around group 8 where the ligand RAO and metal *d* orbitals are roughly equal in energy. Thus, in iminoxolene complexes of ruthenium and osmium, oxidation state assignments are generally attempted but are often ambiguous or unsatisfactory. Descriptions frequently involve resonance structures between multiple oxidation states,<sup>8,9</sup> admissions that compounds are "exceptions to the structural pattern that associates features with localized ligand charge and a defined formal charge for the coordinated metal ion,"<sup>10</sup> or characterizations of bonding as "intricate."<sup>11</sup>

Why not, then, eschew an ionic description and instead use as a starting point a covalent model for the bonding in these complexes? If the metal-ligand  $\pi$  bonding is in fact highly covalent, then describing it as such offers the possibility of a straightforward, intuitive, and general bonding analysis. Here we describe the preparation of a number of chelating bis- and tris-iminoxolene complexes of ruthenium and osmium. The spectroscopic and structural features of these compounds are indeed readily explained by simple covalent bonding models that do not require determination of the metal or ligand oxidation state. By using this covalent picture as a starting point, the similarities between compounds that would be considered as unrelated in an oxidation state picture can be highlighted. As a result, detailed structural analyses of a variety of ruthenium and osmium iminoxolenes can be undertaken to afford insights into the electron distribution in the metal-ligand  $\pi$  bonds.

## Experimental Section

### General procedures

Unless otherwise noted, all procedures were carried out in the air. Reactions run under an inert atmosphere were done in a nitrogen-filled glovebox or on a vacuum line. Deuterated solvents were obtained from Cambridge Isotope Laboratories. 2,2'-Biphenylbis(3,5-di-*tert*-butyl-2-hydroxyphenylamine) (ClipH<sub>4</sub>),<sup>12</sup> tris(2-(3',5'-di-*tert*-butyl-2'-hydroxyphenyl)amino-4-methylphenyl)amine (MeClampH<sub>6</sub>),<sup>5</sup> and OsO(OCH<sub>2</sub>CH<sub>2</sub>O)<sub>2</sub><sup>13</sup> were prepared according to literature procedures. Di- $\mu$ -chlorobis[(*p*-cymene)chlororuthenium(II)] was purchased from Strem Chemicals, while the analogous osmium complex was

prepared from H<sub>2</sub>O<sub>2</sub>Cl<sub>6</sub> and  $\alpha$ -terpinene.<sup>14</sup> All other reagents were commercially available and used without further purification. NMR spectra were measured on a Bruker Avance DPX-400 or -500, or a Varian VXR-500 spectrometer. Chemical shifts are reported in ppm downfield of TMS, with spectra referenced using the chemical shifts of the solvent residuals. Infrared spectra were recorded on a Jasco 6300 FT-IR spectrometer as solids using an ATR plate. UV-visible-NIR spectra were measured as CH<sub>2</sub>Cl<sub>2</sub> solutions in a 1-cm quartz cell on a Jasco V-670 spectrophotometer or on a ThermoFisher Evolution Array diode array spectrophotometer. Mass spectra were measured on a Bruker micrOTOF II spectrometer using electrospray ionization. Elemental analyses were performed by M-H-W Laboratories (Phoenix, AZ, USA).

### Syntheses

**trans-(Clip)Os(py)<sub>2</sub>.** Into a 20-mL screw-cap vial are added 112.9 mg {(*p*-cymene)OsCl<sub>2</sub>}<sub>2</sub> (0.143 mmol), 181.6 mg ClipH<sub>4</sub> (0.3063 mmol, 1.07 equiv per Os), 53  $\mu$ L pyridine (0.658 mmol, 2.3 equiv per Os), 900  $\mu$ L triethylamine, and 10 mL benzene. The vial is sealed with a Teflon-lined cap and heated 18 h in a 70 °C oil bath. After cooling to room temperature, the volatiles are removed on the rotary evaporator and the residue slurried in acetonitrile. Filtration and air-drying gives 61.0 mg *trans*-(Clip)Os(py)<sub>2</sub> (23%). <sup>1</sup>H NMR (C<sub>6</sub>D<sub>6</sub>):  $\delta$  1.37 (s, 18H, <sup>t</sup>Bu), 1.80 (s, 18H, <sup>t</sup>Bu), 5.69 (d, 2 Hz, 2H, ArH), 5.81 (m, 4H, py 4-H + ArH), 5.90 (t, 7 Hz, 4H, py 3,5-H), 6.71 (d, 5 Hz, 4H, py 2,6-H), 7.10 (d, 2 Hz, 2H, ArH), 7.26 (td, 7, 2 Hz, 2H, ArH), 7.33 (dd, 8, 1 Hz, 2H, ArH), 7.62 (dd, 8, 1 Hz, 2H, ArH). <sup>13</sup>C{<sup>1</sup>H} NMR (C<sub>6</sub>D<sub>6</sub>):  $\delta$  30.70, 32.98 (C[CH<sub>3</sub>]<sub>3</sub>), 34.72, 36.31 (C[CH<sub>3</sub>]<sub>3</sub>), 120.50, 122.34, 122.99, 124.08, 124.79, 134.04, 134.09, 134.92, 136.49, 136.71, 137.26, 148.36, 148.90, 161.30 (py 2,6-C), 186.65 (CO). IR (cm<sup>-1</sup>): 2952 (m), 1605 (w), 1586 (w), 1542 (w), 1475 (s), 1451 (s), 1424 (w), 1397 (w), 1385 (w), 1361 (m), 1298 (s), 1271 (w), 1252 (s), 1201 (m), 1171 (w), 1160 (w), 1036 (w), 986 (m), 925 (w), 894 (m), 863 (m), 806 (m), 763 (m), 746 (s), 689 (s). UV-Vis-NIR:  $\lambda_{\text{max}}$  = 1362 nm ( $\epsilon$  = 530 L mol<sup>-1</sup> cm<sup>-1</sup>), 915 (sh, 2500), 718 (23100), 466 (sh, 4900), 400 (10000), 323 (18000). ESI-MS: *m/z* = 938.4156 (M<sup>+</sup>, calcd 938.4175). Anal. Calcd for C<sub>50</sub>H<sub>58</sub>N<sub>4</sub>O<sub>2</sub>Os: C, 64.07; H, 6.24; N, 5.98. Found: C, 66.56; H, 6.76; N, 5.60.

**cis- $\beta$ -(Clip)Os(OCH<sub>2</sub>CH<sub>2</sub>O).** Into a 50 mL Erlenmeyer flask are added 130.4 mg OsO(OCH<sub>2</sub>CH<sub>2</sub>O)<sub>2</sub> (0.400 mmol), 237.4 mg ClipH<sub>4</sub> (0.400 mmol), 10 mL dichloromethane and a magnetic stirbar. The flask is sealed with parafilm and stirred 15 h at room temperature, at which point 51.9 mg additional OsO(OCH<sub>2</sub>CH<sub>2</sub>O)<sub>2</sub> (0.159 mmol, 0.4 equiv) is added and the stirring continued an additional 24 h. The reaction mixture is loaded onto a plug of silica gel and eluted first with CH<sub>2</sub>Cl<sub>2</sub> (to wash out any unreacted ligand and a small amount of a purple byproduct), then 3:1 hexane:ethyl acetate to elute the dark purple product. After the solvent is removed from the eluate on a rotary evaporator, the residue is slurried in 8 mL pentane and suction filtered, washed with 5 mL additional pentane and air-dried 30 min to give 239.3 mg *cis*- $\beta$ -(Clip)Os(OCH<sub>2</sub>CH<sub>2</sub>O) (71%). <sup>1</sup>H NMR (CD<sub>2</sub>Cl<sub>2</sub>):  $\delta$  1.20 (s, 9H, <sup>t</sup>Bu), 1.21 (s, 9H, <sup>t</sup>Bu), 1.29 (s, 9H, <sup>t</sup>Bu), 1.67 (s, 9H, <sup>t</sup>Bu), 4.92 (ddd, 7.6, 4.2, 2.6 Hz,

1H, OCHH'CH''H'''O), 5.71 (ddd, 7.8, 4.6, 2.7 Hz, 1H, OCHH'CH''H'''O), 5.94 (td, 9, 4.4 Hz, 1H, OCHH'CH''H'''O), 6.51 (dd, 8, 1 Hz, 1H, biphenyl 3- or 6-H), 6.88 (d, 2 Hz, 1H, iminoxolene 4- or 6-H), 6.97 (td, 7.5, 1.5 Hz, 1H, biphenyl 4- or 5-H), 7.02 (td, 7.5, 1 Hz, 1H, biphenyl 4- or 5-H), 7.06 (d, 2 Hz, 1H, iminoxolene 4- or 6-H), 7.09 (d, 2 Hz, 1H, iminoxolene 4- or 6-H), 7.17 (dd, 8, 1 Hz, 1H, biphenyl 3- or 6-H), 7.29 (dd, 7.5, 1.5 Hz, biphenyl 3- or 6-H), 7.42 (d, 2 Hz, 1H, iminoxolene 4- or 6-H), 7.47 (td, 8, 1 Hz, 1H, biphenyl 4- or 5-H), 7.56 (td, 8, 1 Hz, 1H, biphenyl 4- or 5-H), 7.64 (dd, 8, 1 Hz, 1H, biphenyl 3- or 6-H), 7.66 (td, 9, 4.7 Hz, 1H, OCHH'CH''H'''O).  $^{13}\text{C}\{^1\text{H}\}$  NMR ( $\text{CD}_2\text{Cl}_2$ ):  $\delta$  30.15, 30.55, 31.32, 31.70 ( $\text{C}[\text{CH}_3]_3$ ), 34.62, 34.93, 35.50, 36.02 ( $\text{C}[\text{CH}_3]_3$ ), 92.24, 93.72 ( $\text{OCH}_2\text{C}'\text{H}_2\text{O}$ ), 110.72, 111.83, 123.05, 124.05, 126.72, 128.07, 128.11, 128.21, 128.23, 129.00, 130.43, 130.98, 133.80, 134.52, 139.83, 142.86, 144.79, 147.04, 150.18, 159.15, 160.02, 161.26, 171.84 (Ar CO), 191.50 (Ar CO). IR ( $\text{cm}^{-1}$ ): 2953 (s), 2910 (m), 2868 (w), 2832 (w), 1636 (w), 1594 (w), 1542 (m), 1476 (m), 1459 (m), 1446 (m), 1426 (m), 1362 (s), 1310 (m), 1251 (m), 1229 (s), 1200 (s), 1170 (s), 1125 (w), 1100 (w), 1033 (s), 1002 (w), 933 (m), 920 (m), 903 (m), 889 (m), 865 (m), 832 (w), 776 (m), 764 (m), 747 (s), 704 (m), 688 (w), 654 (w). UV-Vis-NIR:  $\lambda_{\text{max}} = 1555$  nm ( $\epsilon = 290$  L mol $^{-1}$  cm $^{-1}$ ), 716 (sh,  $\epsilon = 2600$ ), 557 (13900), 417 (6400), 358 (5200). Anal. Calcd for  $\text{C}_{42}\text{H}_{52}\text{N}_2\text{O}_4\text{Os}$ : C, 60.12; H, 6.25; N, 3.34. Found: C, 60.33; H, 6.37; N, 3.47.

**cis- $\beta$ -(Clip)OsCl $_2$ .** Into a 20 mL screw-cap vial is weighed 122.0 mg (Clip)Os( $\text{OCH}_2\text{CH}_2\text{O}$ ) (0.145 mmol). In the glovebox, 5 mL  $\text{CHCl}_3$ , 180  $\mu\text{L}$  chlorotrimethylsilane (1.42 mmol, 10 equiv) and a stirbar are added to the vial, which is then capped securely and stirred in a 60 °C oil bath for 13 h. After cooling to room temperature, the vial is opened to the air and the solvent removed on a rotary evaporator. The dark purple residue is slurried in 2 mL hexane and filtered on a glass frit. After washing with 2  $\times$  2 mL hexane and 2  $\times$  2 mL methanol and air-drying 30 min, the yield of cis- $\beta$ -(Clip)OsCl $_2$  is 87.9 mg (71%).  $^1\text{H}$  NMR ( $\text{C}_6\text{D}_6$ ):  $\delta$  0.95 (s, 9H,  $^t\text{Bu}$ ), 0.98 (s, 9H,  $^t\text{Bu}$ ), 1.36 (s, 9H,  $^t\text{Bu}$ ), 1.76 (s, 9H,  $^t\text{Bu}$ ), 6.13 (dd, 8, 1.5 Hz, 1H, biphenyl 3- or 6-H), 6.37 (td, 7.5, 1.5 Hz, 1H, biphenyl 4- or 5-H), 6.41 (td, 7.5, 1.5 Hz, 1H, biphenyl 4- or 5-H), 6.68 (d, 2 Hz, 1H, iminoxolene 4- or 6-H), 6.88 (td, 7.5, 1.2 Hz, 1H, biphenyl 4- or 5-H), 6.92 (dd, 7.5, 1.5 Hz, 1H, biphenyl 3- or 6-H), 7.10 (td, 7.5, 1.3 Hz, 1H, biphenyl 4- or 5-H), 7.21 (dd, 7.5, 1.3 Hz, 1H, biphenyl 3- or 6-H), 7.25 (dd, 7.5, 1.2 Hz, 1H, biphenyl 3- or 6-H), 7.34 (d, 2 Hz, 1H, iminoxolene 4- or 6-H), 7.40 (d, 2 Hz, 1H, iminoxolene 4- or 6-H), 7.44 (d, 2 Hz, 1H, iminoxolene 4- or 6-H).  $^{13}\text{C}\{^1\text{H}\}$  NMR ( $\text{CD}_2\text{Cl}_2$ ):  $\delta$  30.05, 30.30, 30.95, 31.38 ( $\text{C}[\text{CH}_3]_3$ ), 34.94, 35.07, 35.35, 35.95 ( $\text{C}[\text{CH}_3]_3$ ), 111.14, 111.75, 120.52, 127.69, 128.61, 128.66, 129.62, 130.04, 130.29, 130.63, 131.29, 132.31, 134.36, 134.62, 140.73, 144.54, 148.59, 149.37, 152.38, 159.87, 165.73, 169.19, 187.74 (CO), 203.24 (CO). IR ( $\text{cm}^{-1}$ ): 2953 (m), 2905 (w), 2871 (w), 1596 (w), 1531 (m), 1475 (m), 1462 (m), 1444 (w), 1427 (w), 1388 (w), 1362 (m), 1324 (w), 1292 (w), 1259 (s), 1238 (s), 1201 (m), 1170 (s), 1122 (m), 1106 (w), 1061 (w), 1028 (m), 998 (w), 930 (m), 916 (m), 868

(m), 829 (w), 783 (w), 763 (w), 746 (s), 702 (w), 666 (m), 654 (m). UV-Vis-NIR:  $\lambda_{\text{max}} = 1527$  nm ( $\epsilon = 460$  L mol $^{-1}$  cm $^{-1}$ ), 968 (470), 743 nm (2500), 550 (13100), 500 (sh, 9400), 417 (5200), 359 (sh, 4300). Anal. Calcd for  $\text{C}_{40}\text{H}_{48}\text{Cl}_2\text{N}_2\text{O}_2\text{Os}$ : C, 56.52; H, 5.69; N, 3.30. Found: C, 56.07; H, 5.67; N, 3.39.

**$\kappa^6$ -[Tris(2-(3',5'-di-*tert*-butyl-2'-oxyphenyl)amido-4-methylphenyl)amine]osmium(VI), (MeClamp)Os.** Into a 125 mL Erlenmeyer flask are weighed 0.3401 g (*p*-cymene)OsCl $_2$  $_2$  (0.4301 mmol) and 0.6285 g MeClampH $_6$  (0.6627 mmol, 0.77 equiv per Os). Triethylamine (0.95 mL, 6.8 mmol, 10 equiv per MeClampH $_6$ ) and 40 mL  $\text{CHCl}_3$  are added to the flask to give a purple solution. After stirring the reaction mixture for 1 d, the triethylamine hydrochloride is removed by filtration through Celite. The solvent is evaporated under reduced pressure and the purple residue is triturated with acetonitrile and then suction filtered over a glass frit to yield 0.4370 g (MeClamp)Os as a dark purple solid (58%).  $^1\text{H}$  NMR ( $\text{C}_6\text{D}_6$ ):  $\delta$  1.26 (s, 27H,  $^t\text{Bu}$ ), 1.59 (s, 27H,  $^t\text{Bu}$ ), 1.53 (s, 9H,  $\text{CH}_3$ ), 4.79 (d, 2 Hz, 3H, iminoxolene 4-H), 5.70 (d, 1.5 Hz, 3H, Ar 3-H), 5.88 (ddq, 8, 2, 0.7 Hz, 3H, Ar 5-H), 6.10 (d, 2 Hz, 3H, iminoxolene 6-H), 7.41 (d, 8 Hz, 3H, Ar 6-H).  $^{13}\text{C}\{^1\text{H}\}$  NMR ( $\text{C}_6\text{D}_6$ ):  $\delta$  20.65 ( $\text{CH}_3$ ),  $\delta$  29.31, 31.82 ( $\text{C}(\text{CH}_3)_3$ ), 34.59, 36.21 ( $\text{C}(\text{CH}_3)_3$ ), 112.02, 124.73, 125.93, 131.05, 131.55, 132.45, 134.26, 135.89, 138.37, 139.46, 157.58, 187.03. IR ( $\text{cm}^{-1}$ ): 2959 (w), 2886 (w), 1590 (w), 1542 (m), 1498 (m), 1460 (w), 1402 (w), 1385 (w), 1361 (m), 1317 (m), 1303 (w), 1228 (s), 1188 (s), 1149 (w), 1127 (w), 1108 (m), 1067 (w), 1027 (m), 997 (m), 956 (m), 937 (w), 909 (m), 885 (w), 871 (w), 852 (w), 809 (m), 768 (w), 738 (m), 716 (w), 706 (w), 671 (w). ESI-MS:  $m/z = 1130.5645$  ( $\text{M}^+$ , calcd 1130.5689). UV-Vis-NIR:  $\lambda_{\text{max}} = 1640$  nm (sh,  $\epsilon = 3400$  L mol $^{-1}$  cm $^{-1}$ ), 1354 (6100), 964 (5000), 513 (14900), 376 (13900), 280 (39600). Anal. Calcd for  $\text{C}_{63}\text{H}_{78}\text{N}_4\text{O}_3\text{Os}$ : C, 66.99; H, 6.96; N, 4.96. Found: C, 66.77; H, 7.12; N, 5.13.

**$\kappa^6$ -[Tris(2-(3',5'-di-*tert*-butyl-2'-oxyphenyl)amido-4-methylphenyl)amine]ruthenium(VI), (MeClamp)Ru.** The compound is prepared analogously to the osmium analogue using 0.1238 g (*p*-cymene)RuCl $_2$  $_2$  (0.2022 mmol), 0.3843 g MeClampH $_6$  (0.4052 mmol, 0.95 equiv per Ru) and 0.565 mL triethylamine to give 0.1929 g (MeClamp)Ru (45%).  $^1\text{H}$  NMR ( $\text{C}_6\text{D}_6$ ):  $\delta$  1.32 (s, 27H, 5- $^t\text{Bu}$ ), 1.51 (s, 9H,  $\text{CH}_3$ ), 1.59 (s, 27H, 3- $^t\text{Bu}$ ), 2.05 (s, 3H, iminoxolene 4-H), 4.87 (s, 3H, iminoxolene 6-H), 5.29 (s, 3H, Ar 3-H), 5.50 (sl br d, 8 Hz, 3H, Ar 5-H), 7.73 (d, 8 Hz, 3H, Ar 6-H).  $^{13}\text{C}\{^1\text{H}\}$  NMR ( $\text{C}_6\text{D}_6$ ):  $\delta$  21.75 (Ar $\text{CH}_3$ ), 28.17 ( $\text{C}(\text{CH}_3)_3$ ), 32.94 ( $\text{C}(\text{CH}_3)_3$ ), 34.33 ( $\text{C}(\text{CH}_3)_3$ ), 36.42 ( $\text{C}(\text{CH}_3)_3$ ), 116.69, 119.59, 122.11, 123.45, 130.86, 133.07, 133.42, 140.20, 140.94, 150.41, 176.17, 193.48. IR ( $\text{cm}^{-1}$ ): 2952 (w), 2902 (w), 2862 (w), 1583 (w), 1531 (m), 1495 (m), 1459 (w), 1381 (m), 1359 (m), 1324 (m), 1282 (w), 1297 (s), 1192 (s), 1147 (m), 1125 (m), 1105 (s), 1024 (s), 995 (m), 952 (w), 905 (m), 874 (w), 852 (w), 810 (m), 771 (w), 738 (s), 6.99 (w), 674 (w). ESI-MS:  $m/z = 1040.5151$  ( $\text{M}^+$ , calcd 1040.5117). UV-Vis-NIR:  $\lambda_{\text{max}} = 1860$  nm ( $\epsilon = 2300$  L mol $^{-1}$  cm $^{-1}$ ), 1156 (3200), 583 (16400), 288 (33200). Anal. Calcd for  $\text{C}_{63}\text{H}_{78}\text{N}_4\text{O}_3\text{Ru}$ : C, 72.73; H, 7.56; N, 5.39. Found: C, 72.65; H, 7.81; N, 5.48.

Table 1. Summary of crystal data.

	(Clip)Os(py) <sub>2</sub>	(Clip)OsCl <sub>2</sub> •EtOAc	(MeClamp)Os	(MeClamp)Ru • C <sub>6</sub> D <sub>6</sub>
Molecular formula	C <sub>50</sub> H <sub>58</sub> N <sub>4</sub> O <sub>2</sub> Os	C <sub>44</sub> H <sub>56</sub> Cl <sub>2</sub> N <sub>2</sub> O <sub>4</sub> Os	C <sub>63</sub> H <sub>78</sub> N <sub>4</sub> O <sub>3</sub> Os	C <sub>63</sub> H <sub>78</sub> D <sub>6</sub> N <sub>4</sub> O <sub>3</sub> Ru
Formula weight	937.20	938.00	1129.49	1124.50
<i>T</i> / <i>K</i>	120(2)	120(2)	120(2)	120(2)
Crystal system	Monoclinic	Monoclinic	Monoclinic	Orthorhombic
Space group	<i>P</i> 2 <sub>1</sub> / <i>c</i>	<i>P</i> 2 <sub>1</sub> / <i>n</i>	<i>P</i> 2 <sub>1</sub> / <i>n</i>	<i>Pbca</i>
$\lambda$ /Å	0.71073 (Mo K $\alpha$ )	0.71073 (Mo K $\alpha$ )	0.71073 (Mo K $\alpha$ )	1.54178 (Cu K $\alpha$ )
Total data collected	80737	58745	159593	218296
No. of indep reflns.	11154	8851	14762	12266
<i>R</i> <sub>int</sub>	0.0611	0.0649	0.0932	0.0578
Obsd refls [ <i>I</i> > 2 $\sigma$ ( <i>I</i> )]	9598	7202	11650	11058
<i>a</i> /Å	9.870(7)	11.5267(6)	12.2048(11)	25.7596(3)
<i>b</i> /Å	23.816(19)	10.3290(5)	28.050(3)	17.4114(2)
<i>c</i> /Å	19.126(14)	36.2615(19)	17.3586(16)	27.7512(4)
$\alpha$ /°	90	90	90	90
$\beta$ /°	90.10(2)	98.4471(18)	92.9257(13)	90
$\gamma$ /°	90	90	90	90
<i>V</i> /Å <sup>3</sup>	4496(6)	4270.4(4)	5934.9(9)	12446.7(3)
<i>Z</i>	4	4	4	8
$\mu$ /mm <sup>-1</sup>	2.879	3.153	2.189	2.401
Crystal size/mm	0.31 × 0.10 × 0.07	0.35 × 0.14 × 0.08	0.33 × 0.18 × 0.11	0.16 × 0.11 × 0.10
No. refined params	514	674	951	1016
<i>R</i> 1, <i>wR</i> 2 [ <i>I</i> > 2 $\sigma$ ( <i>I</i> )]	<i>R</i> 1 = 0.0606 <i>wR</i> 2 = 0.1495	<i>R</i> 1 = 0.0280 <i>wR</i> 2 = 0.0557	<i>R</i> 1 = 0.0297 <i>wR</i> 2 = 0.0536	<i>R</i> 1 = 0.0297 <i>wR</i> 2 = 0.0754
<i>R</i> 1, <i>wR</i> 2 [all data]	<i>R</i> 1 = 0.0721 <i>wR</i> 2 = 0.1544	<i>R</i> 1 = 0.0416 <i>wR</i> 2 = 0.0605	<i>R</i> 1 = 0.0472 <i>wR</i> 2 = 0.0573	<i>R</i> 1 = 0.0339 <i>wR</i> 2 = 0.0784
Goodness of fit	1.219	1.009	1.002	1.043

### Electrochemistry

Cyclic voltammetry was performed at a scan rate of 60 mV s<sup>-1</sup> using an Autolab potentiostat (PGSTAT 128N), with glassy carbon working and counter electrodes and a silver/silver chloride reference electrode. The electrodes were connected to the potentiostat through electrical conduits in the drybox wall. Samples were approximately 1 mM in CH<sub>2</sub>Cl<sub>2</sub> with 0.1 M Bu<sub>4</sub>NPF<sub>6</sub> as the electrolyte. Potentials were referenced to ferrocene/ferrocenium at 0 V<sup>15</sup> with the reference potential established by spiking the test solution with a small amount of ferrocene or decamethylferrocene (*E*<sup>o</sup> = -0.565 V vs. Cp<sub>2</sub>Fe<sup>+</sup>/Cp<sub>2</sub>Fe in CH<sub>2</sub>Cl<sub>2</sub><sup>16</sup>).

### Computational methods

Calculations were performed on compounds with all methyl and *tert*-butyl groups replaced by hydrogen atoms. The appropriately pruned solid-state structures were used as starting geometries for optimization using hybrid density functional theory (B3LYP, SDD basis set for ruthenium and osmium and a 6-31G\* basis set for all other atoms), using the Gaussian09 suite of programs.<sup>17</sup> The optimized geometries were confirmed as minima by calculation of vibrational

frequencies. Plots of calculated Kohn-Sham orbitals were generated using Gaussview (v. 5.0.8) with an isovalue of 0.04.

### X-ray crystallography

Crystals of (Clip)OsCl<sub>2</sub>•EtOAc were grown by slow evaporation of a solution of the complex in ethyl acetate/hexane. The other compounds were crystallized by diffusion of CH<sub>3</sub>CN into solutions of the complexes in C<sub>6</sub>H<sub>6</sub> ((Clip)Os(py)<sub>2</sub>), C<sub>6</sub>D<sub>6</sub> ((MeClamp)Ru) or CH<sub>2</sub>Cl<sub>2</sub> ((MeClamp)Os). Crystals were placed in inert oil before transferring to the N<sub>2</sub> cold stream of a Bruker Apex II CCD diffractometer. Data were reduced, correcting for absorption, using the program SADABS. The structures were solved using direct methods. Hydrogen atoms that were placed in calculated positions had their thermal parameters tied to the isotropic thermal parameters of the atoms to which they are bonded (1.5× for methyl, 1.2× for others). Calculations used SHELXTL (Bruker AXS),<sup>18</sup> with scattering factors and anomalous dispersion terms taken from the literature.<sup>19</sup> Further details about the structures are in Table 1.

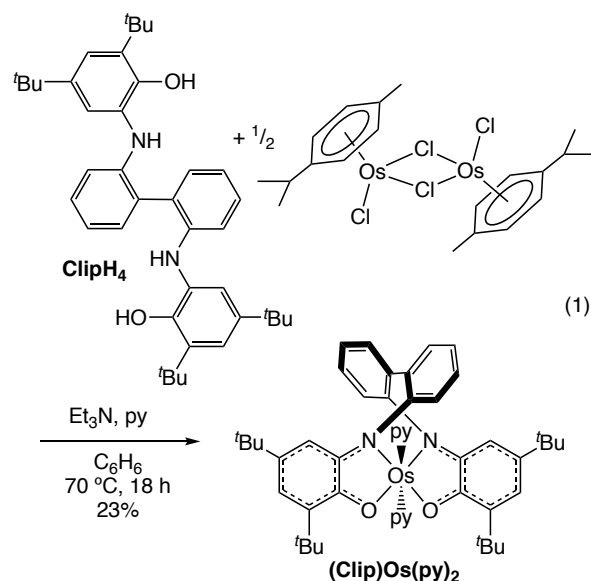
Table 2. Selected bond distances and angles of structurally characterized compounds. Values given are the average of chemically equivalent measurements.

	(Clip)Os(py) <sub>2</sub>	(Clip)OsCl <sub>2</sub> •EtOAc		(MeClamp)Os	(MeClamp)Ru • C <sub>6</sub> D <sub>6</sub>
		<i>n</i> = 1 (N trans to O)	<i>n</i> = 2 (N trans to Cl)		
<i>Bond distances / Å</i>					
M–On	2.049(8)	1.996(2)	2.021(2)	1.998(24)	2.023(7)
M–N <sub>n</sub>	1.973(14)	1.935(3)	1.944(3)	1.984(19)	1.990(5)
On–C <sub>n1</sub>	1.337(9)	1.310(4)	1.303(4)	1.326(3)	1.307(3)
N <sub>n</sub> –C <sub>n2</sub>	1.408(10)	1.360(4)	1.367(4)	1.379(4)	1.353(6)
C <sub>n1</sub> –C <sub>n2</sub>	1.433(10)	1.424(5)	1.422(5)	1.416(3)	1.436(3)
C <sub>n2</sub> –C <sub>n3</sub>	1.398(16)	1.412(5)	1.407(5)	1.397(6)	1.413(2)
C <sub>n3</sub> –C <sub>n4</sub>	1.393(16)	1.362(5)	1.363(5)	1.378(6)	1.372(3)
C <sub>n4</sub> –C <sub>n5</sub>	1.405(14)	1.431(5)	1.426(5)	1.416(5)	1.427(6)
C <sub>n5</sub> –C <sub>n6</sub>	1.401(12)	1.367(5)	1.371(5)	1.389(8)	1.378(3)
C <sub>n1</sub> –C <sub>n6</sub>	1.419(13)	1.414(5)	1.418(4)	1.413(5)	1.426(3)
M–X	2.103(6)	2.3402(9)	2.3176(8)		
M–N10				3.2899(18)	3.3008(14)
Metrical Oxidation State (MOS) <sup>†</sup>	–1.68(13)	–1.12(9)	–1.15(9)	–1.45(5)	–1.07(2)
<i>Bond angles / °</i>					
On–M–N <sub>n</sub>	80.2(4)	78.64(10)	79.16(11)	78.7(8)	78.7(5)
On–M–O( <i>n</i> ±1)	94.2(2)	94.04(9)		92(4)	95.8(11)
N <sub>n</sub> –M–N( <i>n</i> ±1)	105.7(2)	95.07(12)		96.1(13)	95.3(14)
On–M–N( <i>n</i> +1)	173.2(6)	100.58(11)	169.79(10)	95(4)	90.7(5)
On–M–N( <i>n</i> –1)				168(3)	171.9(12)

## Results

### Preparation and characterization of bis- and tris-iminoxolene complexes

Ruthenium(II) and osmium(II) arene complexes are known to react with aminophenols in the presence of bases to give five-coordinate (arene)M(amidophenoxide) complexes.<sup>20</sup> The 2,2'-biphenyl-bridged bis(aminophenol) ligand, 2,2'-(3,5-<sup>t</sup>Bu<sub>2</sub>-2-OH-C<sub>6</sub>H<sub>2</sub>NH)<sub>2</sub>C<sub>12</sub>H<sub>8</sub> (ClipH<sub>4</sub>)<sup>12</sup> also reacts with {(*p*-cymene)OsCl<sub>2</sub>}<sub>2</sub> in the presence of triethylamine under anaerobic conditions to form mixtures of mono- and bis-(cymene)Os complexes, depending on the ligand to osmium ratio employed. Under aerobic conditions in the presence of pyridine, in contrast, the arene ligand is lost and *trans*-(Clip)Os(py)<sub>2</sub> is formed in modest yield (eq 1). The dark green compound is air-stable and diamagnetic, with its NMR spectra confirming that two pyridines are bound per osmium and that the compound has C<sub>2</sub> symmetry. X-ray crystallography (Figure 1) confirms that the *trans* isomer is formed. The *cis*-α and *cis*-β geometries<sup>21</sup> are most commonly observed for octahedral Clip complexes,<sup>22</sup> but the *trans* geometry has been observed in square planar complexes of copper and group 10 metals.<sup>12,23</sup> *Trans*-bis(iminoxolene)osmium complexes with two neutral ligands have not previously been reported, but a *cis* analogue with intramolecular sulfide donors is known,<sup>24</sup> and the *trans*-dioxoleneruthenium complex (Cl<sub>4</sub>C<sub>6</sub>O<sub>2</sub>)<sub>2</sub>Ru(PPh<sub>3</sub>)<sub>2</sub> has been reported.<sup>25</sup>



No products that retain Os–Cl bonds could be isolated from reactions of {(*p*-cymene)OsCl<sub>2</sub>}<sub>2</sub> with ClipH<sub>4</sub>. However, ClipH<sub>4</sub> reacts with the oxoosmium(VI) complex OsO(OCH<sub>2</sub>CH<sub>2</sub>O)<sub>2</sub><sup>13</sup> to replace the oxo group and one of the ethylene glycolate ligands, forming *cis*-β-(Clip)Os(OCH<sub>2</sub>CH<sub>2</sub>O) (eq 2). The NMR spectra of the product unambiguously show the *cis*-β geometry on the basis of the unsymmetrical environments of the Clip ligand and the ethylene glycolate, with the latter showing two inequivalent carbon resonances and four inequivalent proton resonances. The coupling pattern in the

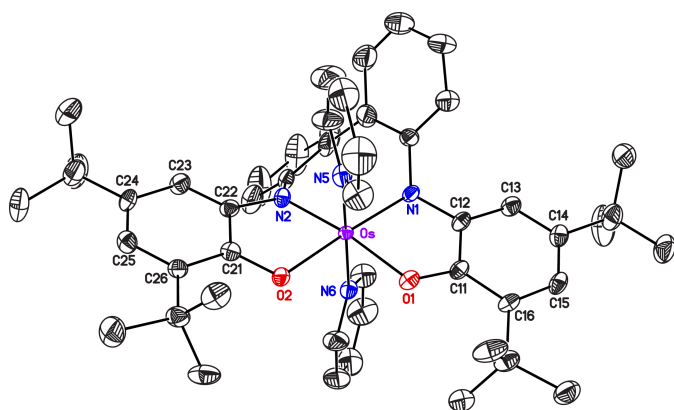
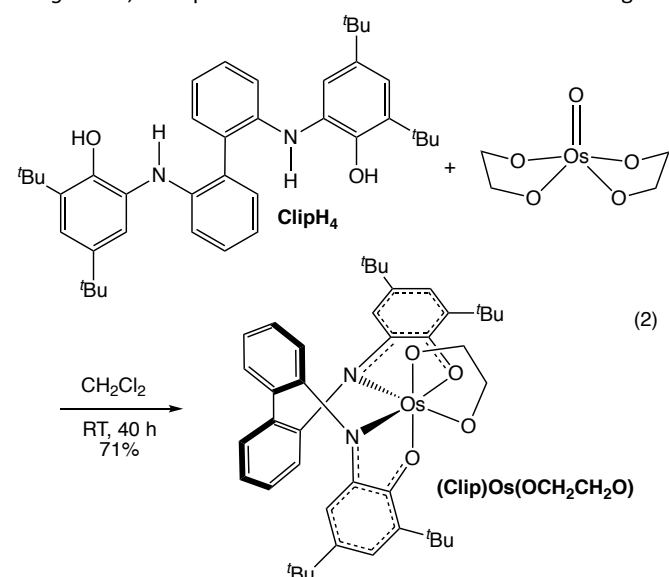


Fig. 1 Thermal ellipsoid plot of *trans*-(Clip)Os(py)<sub>2</sub>, with hydrogen atoms omitted for clarity.

<sup>1</sup>H NMR indicates that the oxygens in the ethylene glycolate are *gauche*, as expected in this five-membered chelate ring.



Heating (Clip)Os(OCH<sub>2</sub>CH<sub>2</sub>O) with chlorotrimethylsilane produces the chloro complex *cis*-β-(Clip)OsCl<sub>2</sub> (eq 3). The same compound is also produced on reaction of ClipH<sub>4</sub> with the osmium(VI) nitride complex (Bu<sub>4</sub>N)[OsNCl<sub>4</sub>], but in lower yields and in the presence of other byproducts that make purification difficult. The *cis*-β stereochemistry is indicated both by the unsymmetrical NMR spectra of the dichloride complex and by its solid-state structure (Fig. 2).

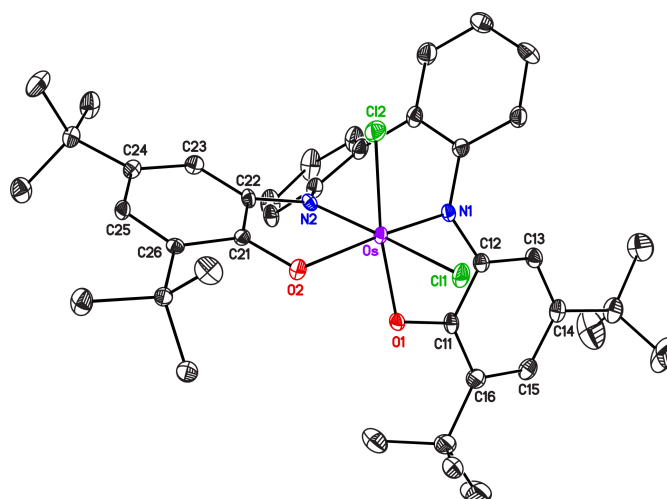
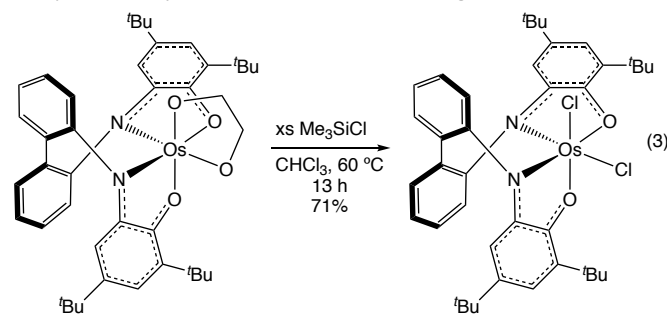
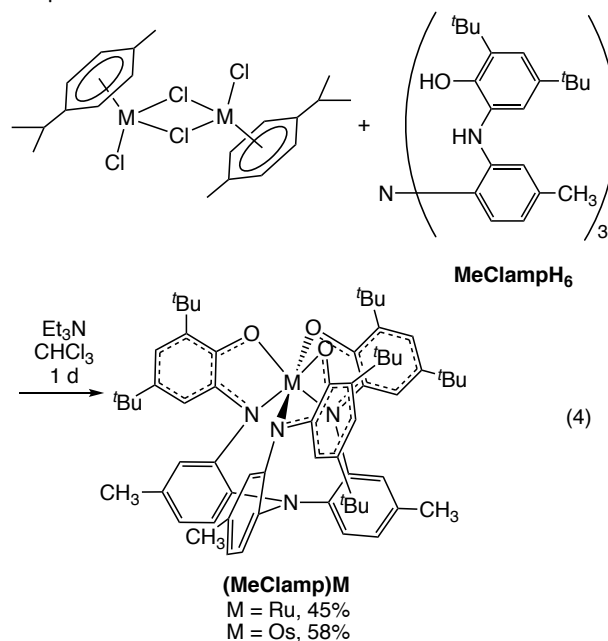
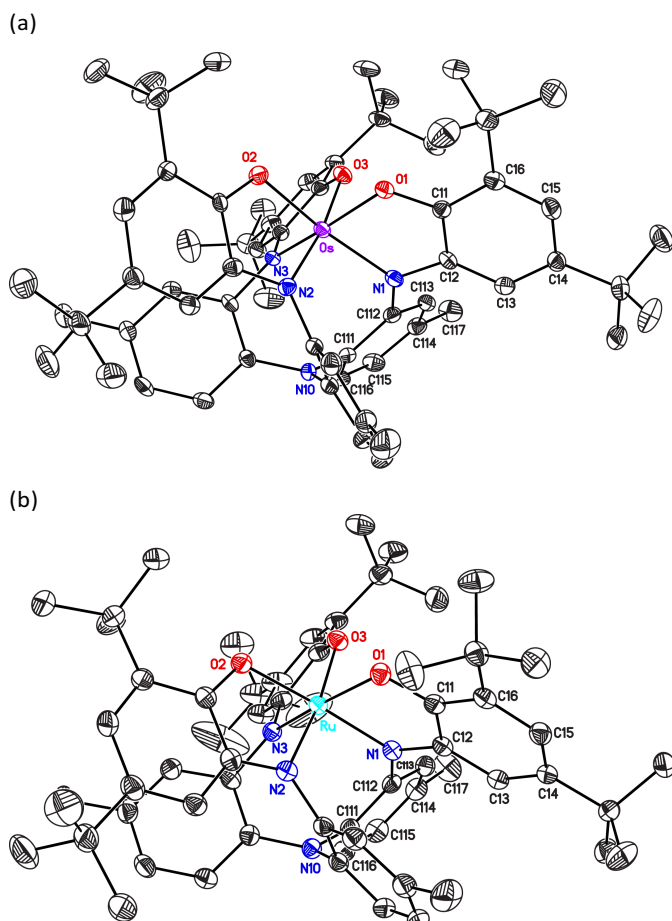


Fig. 2 Thermal ellipsoid plot of *cis*-β-(Clip)OsCl<sub>2</sub>·EtOAc, with lattice solvent and hydrogen atoms omitted for clarity.

The tris(aminophenol) ligand MeClampH<sub>6</sub><sup>5</sup> reacts with both osmium(II) and ruthenium(II) cymene complexes {(*p*-cymene)MCl<sub>2</sub>}<sub>2</sub> in the presence of air and triethylamine to give the encapsulated complexes (MeClamp)M (M = Os, Ru; eq 4). Analogous complexes with unlinked iminoxolene ligands, *mer*-(<sup>Ph</sup>ap)<sub>3</sub>M (<sup>Ph</sup>apH<sub>2</sub> = 2-(*N*-phenylamino)-4,6-di-*tert*-butylphenol), have been prepared previously from MCl<sub>3</sub> and the aminophenol under basic conditions in the air.<sup>26,27</sup>



NMR spectra confirm that the chelated compounds are symmetrical in solution, but do not address the question of whether the central nitrogen atom is coordinated to the metal center (as in (MeClamp)Mo<sup>5</sup>) or not (as in (MeClamp)Ti<sup>28</sup>). X-ray crystallography (Figure 3) indicates that the triarylamine nitrogen does not coordinate to the metal center in either compound ( $d_{M-N} > 3.28$  Å). The metals exhibit fairly regular octahedral geometries and bind the ligands in a *fac* orientation as required by the chelate structure.



**Fig. 3** Thermal ellipsoid plots of (a) (MeClamp)Os and (b) (MeClamp)Ru·C<sub>6</sub>D<sub>6</sub>. Lattice solvent and hydrogen atoms are omitted for clarity.

(MeClamp)Os and (MeClamp)Ru are diamagnetic by Evans method measurements and show sharp <sup>1</sup>H and <sup>13</sup>C NMR spectra. The observed chemical shifts are, however, somewhat shifted from what is expected in diamagnetic compounds. For example, the most upfield resonance of the aromatic protons, assigned on the basis of 2D NMR experiments to the proton between the two *tert*-butyl groups, resonates at  $\delta$  4.79 ppm in (MeClamp)Os and at a remarkable  $\delta$  2.05 ppm in (MeClamp)Ru. One possible explanation for such large chemical shifts is the presence of a low-lying triplet state, where even a thermal population too small to detect directly by magnetic measurements can lead to appreciable changes in the <sup>1</sup>H NMR spectrum.<sup>23,28,29</sup> For example, the tris(diimine)ruthenium complex (ArN=CHCH=NAr)<sub>3</sub>Ru (Ar = 4-CH<sub>3</sub>OC<sub>6</sub>H<sub>4</sub>),<sup>30</sup> which is nominally isoelectronic with (MeClamp)Ru, displays large chemical shifts at ambient temperature but not at -80 °C. However, compounds with thermally populated triplets give rise to temperature-dependent chemical shifts that move nonlinearly away from their diamagnetic values as temperature increases, and the (MeClamp)M complexes show only modest, linear temperature dependences of their chemical shifts. Therefore, the large chemical shifts do not appear to be due to thermal population of a triplet state. We do not currently have a good explanation for these chemical shifts, which are particularly

remarkable as the <sup>1</sup>H NMR spectra of *mer*-(<sup>Ph</sup>ap)<sub>3</sub>M (M = Os, Ru) are reported to show chemical shifts in the normal ranges.<sup>26,27</sup> In a number of other iminoxolene complexes, the <sup>13</sup>C chemical shifts of the C–O *ipso* carbon have been used as a marker of the oxidation state of the iminoxolene ligand, with more downfield chemical shifts corresponding to more oxidized ligands.<sup>31</sup> This correlation does not appear to be applicable to any of the Ru or Os compounds reported here, as all show CO chemical shifts downfield of the ~184 ppm displayed by the fully oxidized free iminoquinones.<sup>6,32</sup>

### Bonding and optical spectroscopy in osmium and ruthenium iminoxolenes

Analysis of the bonding in the bis- and tris-iminoxolene complexes shows that the frontier orbitals are formed from the three osmium *d* $\pi$  orbitals and the redox-active orbitals (RAOs) of the iminoxolene ligands (Fig. 4). The triarylamine nitrogen-centered nonbonding orbital in (MeClamp)M is similar in energy but is not involved in the bonding or spectroscopy and will not be discussed further.

In a *trans* bis-iminoxolene complex such as (Clip)Os(py)<sub>2</sub>, one of the two RAO combinations (of *B* symmetry in the C<sub>2</sub> point group of (Clip)Os(py)<sub>2</sub>) is approximately symmetric with respect to inversion about the center of the octahedron and so has little overlap with any of the *d* orbitals and is essentially nonbonding. The *A*-symmetry RAO combination interacts strongly with one of the Os *d* $\pi$  orbitals to form a filled bonding and an empty antibonding combination of molecular orbitals (Fig. 4a). This situation is entirely analogous to that seen in square planar group 10 complexes such as (<sup>t</sup>BuClip)Pt.<sup>23</sup> In the Pt complex, the filled metal-centered orbitals are well below the RAO-based orbitals in energy, but the less electronegative Os has two metal-centered orbitals close in energy to the *B*-symmetry RAO combination. The *B*-symmetry *d*<sub>*yz*</sub> orbital has little overlap with the RAO combination, but is so close in energy that it mixes substantially in the ground state. (This orbital is somewhat higher in energy than the *A*-symmetry *d*<sub>*x*<sup>2</sup>-*y*<sup>2</sup></sub> orbital, probably because it is somewhat antibonding with respect to the lower-lying iminoxolene  $\pi$  orbital, the so-called subjacent orbital (SJO). This orbital has previously been observed to have significant effects on the electronic structure of Ru and Os compounds.<sup>33</sup>)

On going from (Clip)OsL<sub>2</sub> (L = py) to (Clip)OsX<sub>2</sub> (X<sub>2</sub> = OCH<sub>2</sub>CH<sub>2</sub>O or Cl<sub>2</sub>), two changes are noteworthy: The latter complexes have two fewer valence electrons (iminoxolene plus metal) than the former, and the geometry changes from *trans* to *cis*. These changes are correlated. Unlike in the *trans* geometry, where only one iminoxolene-metal  $\pi$  bond is possible, in the *cis* geometry two ligand RAO-metal *d* $\pi$  interactions are possible, with the third *d* $\pi$  orbital being nonbonding (Fig. 4b). This bonding situation has been described in detail for the isoelectronic *cis*-(*acac*)<sub>2</sub>TiX<sub>2</sub> structure.<sup>34</sup> In *cis*-(iminoxolene)<sub>2</sub>OsL<sub>2</sub> (L = neutral ligand), one pair of electrons would occupy a metal-ligand  $\pi^*$  orbital, leaving the overall  $\pi$  bond order unchanged at 1. Avoiding antibonding interactions still provides a significant driving force favoring the *trans*

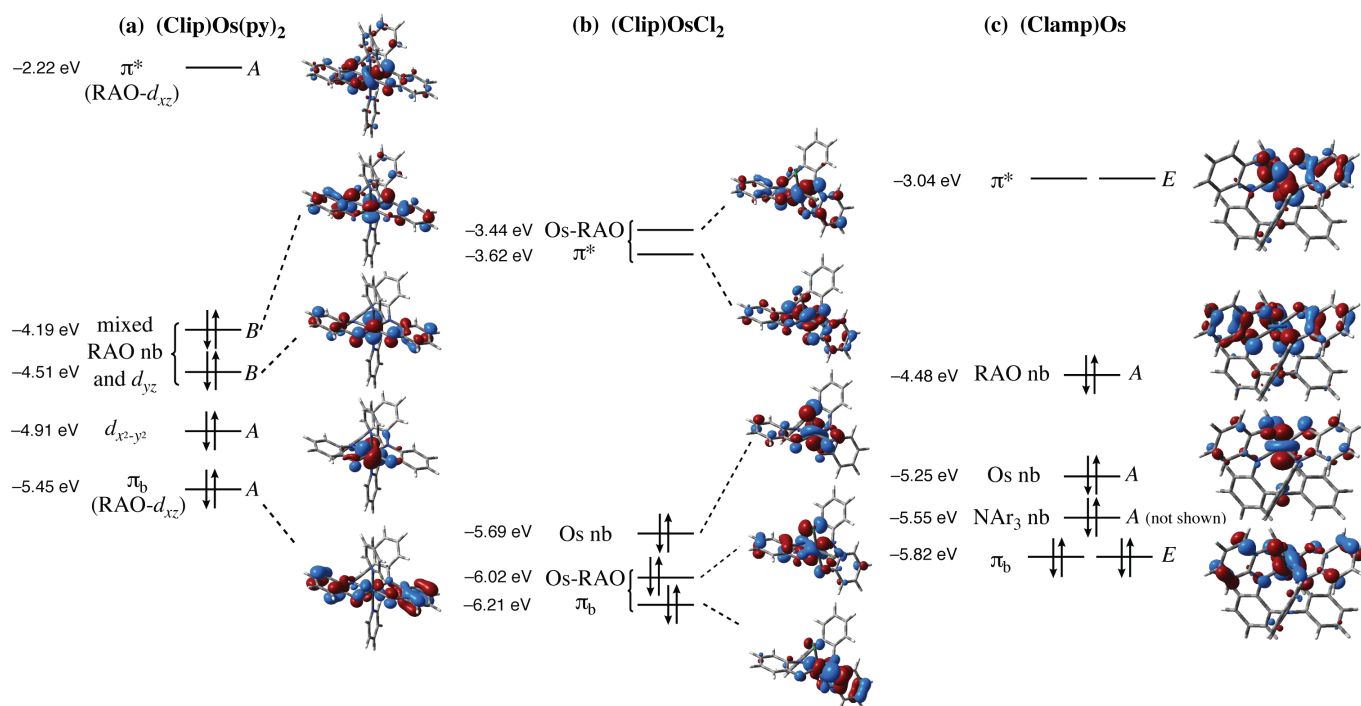


**Fig. 4** Frontier molecular orbital diagrams of (a) *trans*-(Clip)Os(py)<sub>2</sub>; (b) *cis*-β-(Clip)OsCl<sub>2</sub>; and (c) (Clamp)Os. Energies and pictures of Kohn-Sham orbitals are from DFT calculations (B3LYP, SDD basis set for Os, 6-31G\* basis for all other atoms). Aryl groups have hydrogen atoms in place of methyl and *tert*-butyl groups.

geometry, with DFT calculations predicting that *cis*-β-(Clip)Os(py)<sub>2</sub> is 12.5 kcal mol<sup>-1</sup> less stable than the *trans* isomer. But computationally, this preference is overruled, for example, in (Clip)Os(CO)<sub>2</sub> by the superior backbonding in the *cis*-α isomer, which is now calculated to be 5 kcal mol<sup>-1</sup> more stable than the *trans* isomer. Experimentally, both *cis* and *trans* isomers are known for compounds with this electronic structure; for example, both *trans*-(Cl<sub>4</sub>C<sub>6</sub>O<sub>2</sub>)<sub>2</sub>Ru(PPh<sub>3</sub>)<sub>2</sub><sup>25</sup> and its *cis* isomer<sup>35</sup> have been prepared. In contrast, (Clip)OsX<sub>2</sub> would have a π bond order of 2 in the *cis* configuration and only 1 in the *trans* configuration. There is thus a strong preference for the *cis* structure, with DFT calculations indicating that *trans*-(Clip)OsCl<sub>2</sub> is 4.5 kcal mol<sup>-1</sup> less stable than the *cis*-β isomer. Bonding in (MeClamp)M complexes follows the general pattern previously described for M = Mo<sup>5,6</sup> and Ti<sup>28</sup>, with two π bonds and one nonbonding *d*π orbital which overlaps minimally with the A-symmetry combination of ligand RAOs. The presence of two additional valence electrons in the group 8 complexes compared to (MeClamp)Mo leads to occupation of the nonbonding *d*π orbital (essentially *d*<sub>z</sub><sup>2</sup>) and prevents formation of a bond between the triarylamine nitrogen and the metal center. This bonding picture is similar to that given for *mer*-(<sup>Ph</sup>ap)<sub>3</sub>Ru and *mer*-(<sup>Ph</sup>ap)<sub>3</sub>Os.<sup>26</sup>

The optical spectra of the complexes (Fig. 5) support these bonding analyses. In general, weak transitions are seen in the red to near-infrared region of the spectrum for *n*→π\* transitions and intense transitions in the middle of the visible region for π→π\* transitions (Table 3). The optical spectrum of (Clip)Os(py)<sub>2</sub> (Fig. 5a) is dominated by a relatively narrow, very intense transition in the red (λ<sub>max</sub> = 718 nm, ε = 23100 L mol<sup>-1</sup> cm<sup>-1</sup>), similar to what is observed from the analogous

(<sup>t</sup>BuClip)Pt (861 nm, 52100 L mol<sup>-1</sup> cm<sup>-1</sup>).<sup>23</sup> Time-dependent DFT calculations indicate that the excited state corresponding to the intense band at 718 nm is due to promotion of an electron from the ligand-centered B-symmetry orbital to the A-symmetry π\* LUMO (λ<sub>v,max,calc</sub> = 661 nm). The transition from the metal-centered orbital is predicted to be both much weaker and at much lower energy (λ<sub>v,max,calc</sub> = 1156 nm), and is assigned to the broad band at 1380 nm (ε = 520 L mol<sup>-1</sup> cm<sup>-1</sup>).

Table 3. Selected features of the optical spectra of Os and Ru iminoxolenes.

Compound	λ <sub>max</sub> / nm (ε / L mol <sup>-1</sup> cm <sup>-1</sup> ), exptl	λ <sub>max</sub> / nm, TDDFT	Assignment
(Clip)Os(py) <sub>2</sub>	1362 (530)	1156	<i>d</i> <sub>yz</sub> → π*
	718 (23100)	661	RAO nb → π*
(Clip)OsCl <sub>2</sub>	1527 (460)	1331	<i>d</i> <sub>yz</sub> → π*
	968 (470)	1067	<i>d</i> <sub>yz</sub> → π*
	743 (2500)	826	π → π*
	550 (13100)	573	π → π*
	500 (sh, 9400)	568	π → π*
(MeClamp)Os	1354 (6100)	1432	RAO nb → π*
	964 (5000)	1021	<i>d</i> <sub>z</sub> <sup>2</sup> → π*
	513 (14900)	553	π → π*
(MeClamp)Ru	1860 (2300)	1700	RAO nb → π*
	1156 (3200)	1055	<i>d</i> <sub>z</sub> <sup>2</sup> → π*
	583 (16400)	599	π → π*

The (Clamp)M complexes also show excitations from both the ligand- and metal-centered nonbonding orbitals to the π\* orbitals, but here the intensities are much more similar to each other and the difference in energies is not as great, with the *d*<sub>z</sub><sup>2</sup> → π\* transition actually occurring at higher energy. As was observed in (<sup>Ph</sup>ap)<sub>3</sub>M, the excitations in the Os compound occur at higher energies than the corresponding Ru

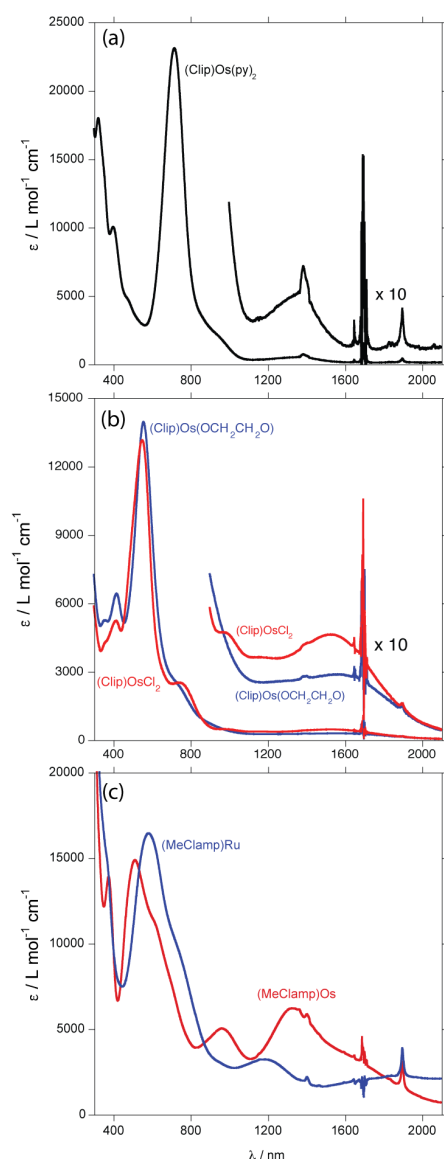


**Fig. 5** Optical spectra in  $\text{CH}_2\text{Cl}_2$  of (a) *trans*-(Clip)Os(py)<sub>2</sub>; (b) *cis*- $\beta$ -(Clip)OsX<sub>2</sub> (X<sub>2</sub> = OCH<sub>2</sub>CH<sub>2</sub>O, Cl<sub>2</sub>); (c) (MeClamp)M (M = Ru, Os). For (a) and (b), the near-IR spectra are also shown magnified tenfold to make the weak NIR features clearer.

compound, though the appearance of the congeners' spectra are qualitatively quite similar.

#### Electrochemistry of osmium and ruthenium iminoxolenes

All of the compounds show rich electrochemistry (Fig. 6). Of note in the cyclic voltammetry of (Clip)Os(py)<sub>2</sub> is the facile oxidation at  $-0.49$  V vs.  $\text{Cp}_2\text{Fe}^+/\text{Cp}_2\text{Fe}$  (Table 4), which occurs at a much lower potential than is typical for iminoxolene-based oxidations (e.g.,  $0.24$  and  $0.78$  V for  $(^t\text{BuClip})\text{Pt}^{23}$ ). DFT calculations suggest that the radical is delocalized over both metal and ligand (Fig. S1), consistent with the close energies of the two orbitals in the neutral compound (Fig. 4a).

In contrast, both the low-potential first oxidations of the (MeClamp)M complexes and their second oxidations are assigned to removal of electrons from the ligand-centered

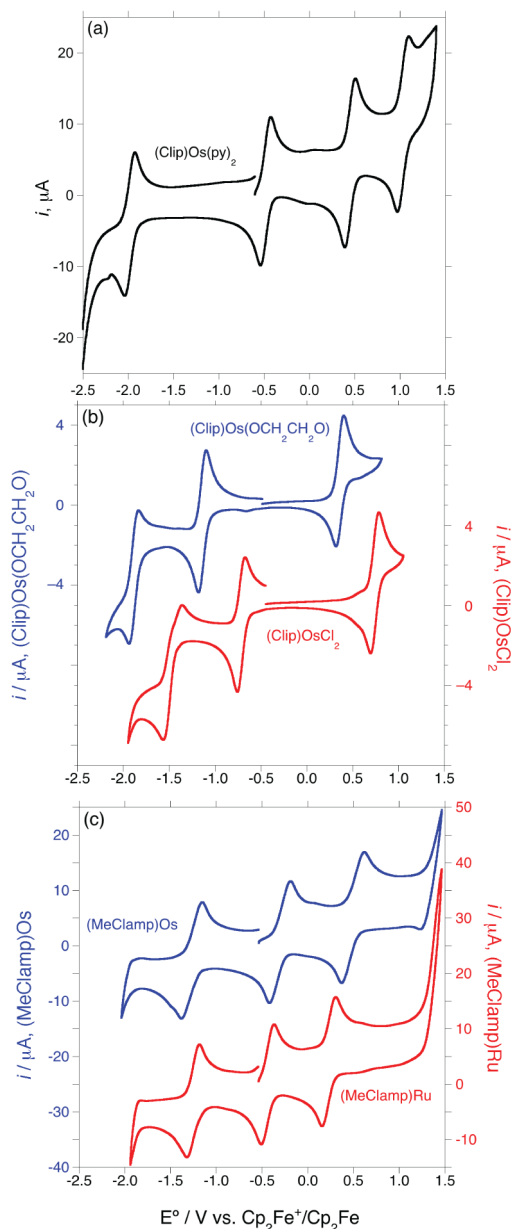


**Fig. 6** Cyclic voltammograms ( $\text{CH}_2\text{Cl}_2$ ,  $0.1$  M  $\text{Bu}_4\text{NPF}_6$ ,  $60$   $\text{mV s}^{-1}$ ). (a) (Clip)Os(py)<sub>2</sub>. (b) *cis*- $\beta$ -(Clip)OsX<sub>2</sub> (X<sub>2</sub> = OCH<sub>2</sub>CH<sub>2</sub>O, Cl<sub>2</sub>). (c) (MeClamp)M (M = Ru, Os).

Table 4. Redox potentials of bis- and tris-iminoxolene complexes of osmium and ruthenium. Data are from cyclic voltammograms in  $\text{CH}_2\text{Cl}_2$  with  $0.1$  M  $(\text{Bu}_4\text{N})\text{PF}_6$  except as noted.

Compound	$E^\circ$ / V vs. $\text{Cp}_2\text{Fe}^+/\text{Cp}_2\text{Fe}$				
	Red 2	Red 1	Ox 1	Ox 2	Ox 3
<i>trans</i> -(Clip)Os(py) <sub>2</sub>		-1.98	-0.49	0.46	1.04
<i>cis</i> - $\beta$ -(Clip)Os(OCH <sub>2</sub> CH <sub>2</sub> O)	-1.88	-1.13	0.36		
<i>cis</i> - $\beta$ -(Clip)OsCl <sub>2</sub>	-1.46	-0.71	0.75		
(MeClamp)Os		-1.30	-0.31	0.49	
(MeClamp)Ru		-1.24	-0.44	0.23	
<i>mer</i> -( <sup>Ph</sup> ap) <sub>3</sub> Os <sup>a</sup>	-2.00	-1.23	-0.16	0.60	
<i>mer</i> -( <sup>Ph</sup> ap) <sub>3</sub> Ru <sup>a,b</sup>	<i>irrev.</i>	-1.14	-0.30	0.40	

<sup>a</sup>Ref. 26. <sup>b</sup>In  $\text{CH}_3\text{CN}/0.1$  M  $(\text{Et}_4\text{N})\text{ClO}_4$ .

nonbonding orbital (the HOMOs of both complexes). The analogous oxidations of the nonchelating <sup>Ph</sup>ap ligand have

been securely assigned to ligand-centered processes on the basis of the EPR spectra of the corresponding radical cations.<sup>26</sup> This is entirely consistent with the orbital energy picture of Fig. 4, where the ligand-centered nonbonding orbital is substantially higher than the metal-centered orbital in (MeClamp)M but of similar energy in (Clip)Os(py)<sub>2</sub>. In (Clip)OsX<sub>2</sub>, there is no ligand-centered nonbonding orbital and the metal-centered nonbonding orbital is at rather low energy. Consequently, these compounds show oxidations at only relatively high potentials, with the waves for the dichloride complex shifting anodically by ~400 mV relative to those of the ethylene glycolate, consistent with the more electron-withdrawing character of chloride. In all cases, reductions presumably take place by additions of electrons into metal-iminoxolene  $\pi^*$  orbitals, and in no cases are metal-iminoxolene  $\pi$  bonding electrons removed at accessible potentials.

A comparison of the redox potentials of the ruthenium and osmium complexes of the MeClamp ligand indicates that the Os compound is both more difficult to reduce (by 60 mV) and more difficult to oxidize (by ~150 mV) than its Ru analogue. The same trend is observed between (<sup>Ph</sup>ap)<sub>3</sub>Os and (<sup>Ph</sup>ap)<sub>3</sub>Ru.<sup>26</sup> For metal-centered redox waves, one would expect Os compounds to be more easily oxidized (and more difficult to reduce) than Ru compounds. This matches with the trend observed in the reduction waves, though since this wave involves a metal-ligand  $\pi^*$  orbital, the stronger bonding expected for the 5d metal may be more germane. But the differences in oxidation waves is surprising, in that it goes in the opposite direction expected for metal-centered redox events and is larger in magnitude than the difference in the reduction waves, despite the fact that the redox event involves a ligand-centered nonbonding orbital. The potential difference may arise from the structural changes in the intraligand bonds on going from Os (MOS = -1.45(5)) to Ru (MOS = -1.07(2)). A more negative metrical oxidation state corresponds to a geometry of the iminoxolene that will lower the energy of the redox-active orbital (e.g., longer C–O and C–N bonds, which will decrease the effect of the carbon-heteroatom antibonding interactions) and hence make removal of electrons from the RAO more difficult. Note that (MeClamp)Mo, whose first oxidation likewise corresponds to removal of an electron from the A-symmetry combination of ligand RAOs, has both a more negative MOS that either of the group 8 compounds (-1.52(9)) and a more positive redox potential (-0.17 V vs. Cp<sub>2</sub>Fe<sup>+</sup>/Cp<sub>2</sub>Fe).<sup>5</sup> DFT calculations on (Clamp)M (M = Ru, Os) indicate that the Kohn-Sham LUMO of the Ru compound is 0.12 eV lower in energy, and the Kohn-Sham HOMO 0.17 eV higher in energy, than the corresponding orbitals of the Os compound, consistent with both the direction and magnitude of the trends observed in the cyclic voltammetry.

## Discussion

### Covalent vs. ionic descriptions of bonding in osmium and ruthenium iminoxolenes

The bonding, structure, and spectroscopy of the bis- and tris-iminoxolene complexes of ruthenium and osmium have been described above in a way that foregrounds the metal-iminoxolene  $\pi$  bonding to provide a generally applicable view of all the compounds. For example, the observation of a *cis* geometry for (Clip)OsCl<sub>2</sub> and a *trans* geometry for (Clip)Os(py)<sub>2</sub> is congruent with the possibility of forming two  $\pi$  bonds in a *cis* octahedral complex in the former compound, while in the latter compound the presence of two additional electrons would require the occupation of a metal-ligand  $\pi^*$  orbital. The diamagnetism of all the isolated compounds is consistent with an arrangement where all bonding and nonbonding orbitals are filled and all antibonding (including  $\pi^*$ ) orbitals are empty; this is equivalent to saying that the compounds obey the 18-electron rule. Electrochemically, the electrons in metal- or ligand-centered nonbonding orbitals are easily removed, but those in  $\pi$  bonding orbitals are not. Optical spectra are readily interpreted in terms of lower-energy  $n \rightarrow \pi^*$  transitions of variable intensity and highly intense  $\pi \rightarrow \pi^*$  transitions.

No attempt has been made to assign formal oxidation states to the ligands or the metals. One could, of course, make such an attempt, but a number of features suggest that the effort would lead to unwieldy descriptions of electronic structure that would not afford additional insights. Consider, for example the tris(iminoxolene) complexes (MeClamp)M (M = Ru, Os). The analogous unlinked complex *mer*-(<sup>Ph</sup>ap)<sub>3</sub>Ru has been described in the literature as a Ru(III) tris-iminosemiquinone.<sup>27</sup> This is in good agreement with the intraligand bond distances (for (MeClamp)Ru, MOS = -1.07(2)) and the observed high symmetry of the structure. However, this formulation requires a complex coupling scheme involving both metal-ligand and ligand-ligand antiferromagnetic coupling to achieve an  $S = 0$  state from the inevitably  $S = 1/2$  octahedral Ru(III) center and three  $S = 1/2$  organic ligand radicals. To make matters worse, the intraligand bond distances in (MeClamp)Os indicate that the ligands are markedly more reduced (MOS = -1.45(5)), suggesting an oxidation state of Os(IV) (as was assigned in *mer*-(<sup>Ph</sup>ap)<sub>3</sub>Os<sup>26</sup>). This gives rise to a simpler coupling scheme (antiferromagnetic coupling between  $S = 1$  Os and the two  $S = 1/2$  ligands) but requires an explanation for the observed symmetry of the structure. Even less satisfactorily, it would suggest a qualitatively different electronic structure for the congeners, flying in the face of their clearly analogous spectroscopic and electrochemical characteristics.

Even features that seem at first glance to be well described by a charge-localized picture are, upon careful consideration, better described by a delocalized model. For example, (Clip)Os(py)<sub>2</sub> would likely be described in a charge-localized model as a mixed semiquinone-amidophenoxide based on its MOS of -1.68(13). The appearance of a broad, weak absorption feature in the near-IR spectrum could be interpreted in terms of the presence of an intervalence transition, consistent with the mixed ligand oxidation states. Yet (Clip)OsCl<sub>2</sub>, which in a charge-localized picture must surely be considered a bis-iminosemiquinone (MOS = -1.12(9), -1.15(9)), has a very similar near-IR feature despite lacking a

mixed-valent ligand set. A molecular orbital analysis suggests that in both cases these bands are due to similar transitions from metal nonbonding  $d$  orbitals to metal-iminoxolene  $\pi^*$  orbitals.

#### General implications of a covalent description of the $\pi$ bonding in osmium and ruthenium iminoxolenes

A great advantage of adopting a covalent picture for these complexes is that it emphasizes the points of similarity among osmium and ruthenium iminoxolene complexes rather than their differences. One certainly could describe them as charge-localized structures; a resonance hybrid of Os(II)-iminoquinone/antiferromagnetically coupled Os(III)-iminoquinone/Os(IV)-amidophenoxide is essentially equivalent to a molecular orbital description of a compound with a filled Os-iminoxolene  $\pi$  bonding orbital. But the valence bond language obscures the similarities among complexes of different nominal oxidation states. In the language of molecular orbital theory, the Os-iminoxolene interaction is essentially similar in nature in different compounds.

While the nature of the  $\pi$  interaction is general, it is tuned in any particular compound by two factors: the geometry of the complex, which alters which  $\pi$  orbitals are bonding, nonbonding, or antibonding; and the total number of  $\pi$  electrons (from the combination of metal  $d$  orbitals and ligand RAOs), which affects which orbitals are occupied and which are empty. The effect of these modulations on the overall metal-iminoxolene  $\pi$  bonding can be summarized by a  $\pi$  bond order. Thus, in a *cis*-bis-iminoxolene such as (Clip)OsCl<sub>2</sub>, both RAO combinations can interact with metal  $d\pi$  orbitals (Fig. 4b), giving rise to two bonding, two antibonding, and one nonbonding (metal-based) orbital. With six electrons, the  $\pi$  bond order is 1, since both  $\pi$  bonding orbitals (and no  $\pi^*$  orbitals) are filled. In a *trans* complex, the *ungerade* RAO combination finds no symmetry match among the metal  $d$  orbitals, giving rise to a single bonding-antibonding pair and three nonbonding orbitals (two metal-centered, one ligand-centered). In (Clip)Os(py)<sub>2</sub>, with 8 total  $\pi$  electrons, this leads to a  $\pi$  bond order of 0.5, since again all the bonding and nonbonding levels are filled and the antibonding levels are empty, giving one  $\pi$  bond spread over two iminoxolene ligands. (A putative *cis* isomer, similar to known (ArNC<sub>6</sub>H<sub>2</sub><sup>t</sup>Bu<sub>2</sub>O)<sub>2</sub>Ru(bpy),<sup>36</sup> would have the same bond order, with two filled bonding and one filled antibonding orbital appropriate to 8  $\pi$  electrons in a *cis* geometry.) Finally, in (MeClamp)M, the  $E$  orbitals form a pair of bonding and a pair of antibonding orbitals, while the two  $A$  symmetry orbitals are essentially nonbonding. Combining this orbital picture with the 8  $\pi$  electrons in the neutral Ru and Os complexes yields a  $\pi$  bond order of 0.67 (two  $\pi$  bonds delocalized over three iminoxolenes).

If  $\pi$  bonding in the group 8 iminoxolenes is highly covalent, then the metrical oxidation states of the ligands should be controlled by the extent of  $\pi$  bonding. If all ligand-centered nonbonding orbitals are filled (which is the case in all Ru and Os compounds that have been structurally characterized so far), then increasing  $\pi$  bonding shifts the electron density in

the ligand RAO increasingly toward the metal. A  $\pi$  bond order of zero corresponds to a filled, fully ligand-localized RAO, and hence a metrical oxidation state of  $-2$ . At the other extreme, a  $\pi$  bond order of one corresponds to that pair of electrons occupying a metal-ligand bonding orbital that is shared between the two, resulting in a decrease in electron density on the ligand and a change in intraligand bond distances equivalent to (partial) ligand oxidation. This correlation is indeed observed in iminoxolene-ruthenium and osmium complexes (Fig. 7; see Tables S1-S2 for a complete listing of examples for which structural data are available). The degree of electron transfer in the bonding orbital is reflected in the slope of this plot. For example, if the bonding orbital were completely localized on the metal, a  $\pi$  bond would be equivalent to transfer of two electrons, and the slope of the plot would be 2. A nonpolar covalent (i.e., equal sharing) bonding interaction would correspond to a slope of 1. For both Ru and Os, the slopes are close to 1, consistent with a high degree of covalency, but there are differences between the metal, with the slope of 1.32 for Ru corresponding to a  $\pi$  bond that is 66% on the metal and 34% on the ligand, while the Os-iminoxolene  $\pi$  bond is polarized in the opposite direction (42% Os/58% ligand). This suggests that the iminoxolene RAO orbital energies are slightly higher in energy than the Os  $5d\pi$  orbitals and slightly lower in energy than the Ru  $4d\pi$  orbitals. These relative orbital energies of the  $4d$  and  $5d$  metals are in line with established periodic trends.<sup>37</sup>

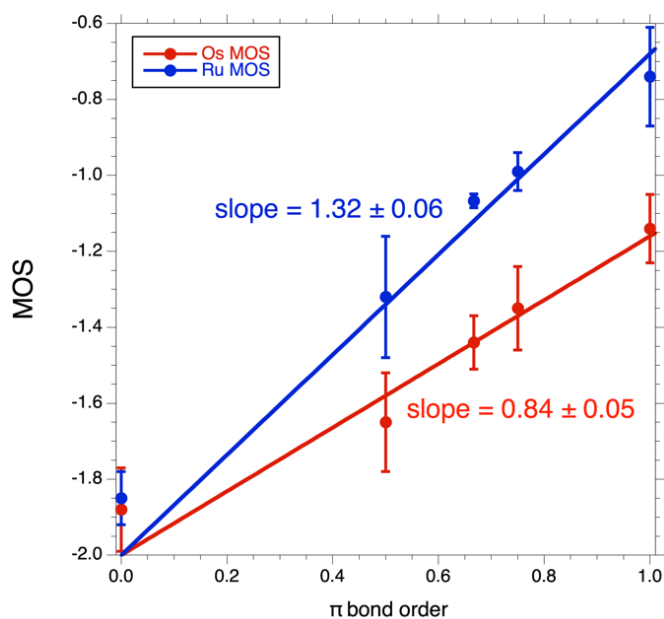


Fig 7 Correlation of metrical oxidation state (MOS) with  $\pi$  bond order in iminoxolene complexes of ruthenium (blue) and osmium (red).

It is worth noting that framing the bonding in terms of polar covalency in this manner clearly illuminates trends in a way that is obscured if one focuses instead on formal ligand oxidation state. Thus, the structures of all the ruthenium iminoxolenes that show any  $\pi$  bonding at all fall in a range that would have them be considered as iminoquinones; a number of researchers have noted the remarkable persistence

of this apparent oxidation state in Ru compounds.<sup>27</sup> But this apparent similarity in fact masks considerable variation in structure (a difference of 0.58 in metrical oxidation state from a  $\pi$  bond order of 0.5 to a  $\pi$  bond order of 1) that is quantitatively accounted for in the covalent picture. Viewed through this lens, it is also possible that the ubiquity of the apparent iminosemiquinone oxidation state in ruthenium chemistry is an artifact of the range of accessible  $\pi$  bond orders and the slight metal-centeredness of the bonding in ruthenium complexes, which conspire to center the range of MOS values around  $-1.0$ . The analogous osmium compounds, with more ligand-heavy bonding, happen to be centered at  $-1.4$ , not particularly close to an integer and hence attracting no physical interpretation. In the covalent picture, the two metals can be seen as entirely analogous.

It is important to recognize the limits of this analysis. One important limitation is that it neglects the effects of the ancillary ligands. In particular, if there are significant  $\pi$  interactions between the ancillary ligands and the orbitals involved in  $\pi$  bonding to the iminoxolenes, it will affect the energy of those orbitals and thus tune the polarity of the metal-iminoxolene  $\pi$  bond. The bis(2-phenylazopyridine) complexes  $(^R\text{ap})\text{Os}(\text{pap})_2$ <sup>38</sup> provide a good example of this. Since 2-phenylazopyridine is isoelectronic with an iminoquinone,  $(^R\text{ap})\text{Os}(\text{pap})_2$  is isoelectronic with  $(\text{MeClamp})\text{Os}$ , but how the  $\pi$  bonding will be distributed between the iminoxolene and phenylazopyridine ligands is unclear. The observed MOS of the iminoxolenes in  $(^R\text{ap})\text{Os}(\text{pap})_2$  ( $-1.56(11)$ , averaged over four examples) is similar to that observed in  $(\text{MeClamp})\text{Os}$  ( $-1.45(5)$ ), indicating that the pap and  $^R\text{ap}$  ligands participate similarly in  $\pi$  bonding, but that would not be predictable *a priori*. An analogous situation is found in  $(\text{arene})\text{Ru}(^R\text{ap})$  complexes, where  $\pi$  bonding from the iminoxolene must compete with bonding to the  $\eta^6$  arene. The average MOS observed ( $-1.60(5)$ , nine examples) suggests that the filled ruthenium-iminoxolene  $\pi$  bonding orbital is mostly, but not entirely, ligand in character. The effect of ancillary ligands on ruthenium-benzoquinonediimine  $\pi$  bonding has been documented,<sup>39</sup> and such ancillary ligand effects doubtless contribute to the significant spread in observed MOS values among compounds with the same nominal  $\pi$  bond order.

A second limitation of this covalent model of  $\pi$  bonding is that, unsurprisingly, it does not work well for compounds whose bonding is much more ionic. In particular, high-spin first-row transition metal complexes do not adhere well to the predictions of the covalent model. For example, the tris(iminoxolene)iron compounds  $(^R\text{ap})_3\text{Fe}$  in all but one case have  $S = 1$  ground states with long Fe-ligand bond lengths that are not conducive to good  $\pi$  overlap.<sup>40-43</sup> A covalent model would incorrectly predict a lower spin state (as found for the Ru and Os compounds), while the experimental observations are well accounted for by a simple ionic model involving high-spin ( $S = 5/2$ ) iron(III) antiferromagnetically coupled to three iminosemiquinone ligand radicals. Even among first-row metals, it is worth noting that there are likely examples of low-spin compounds where a covalent model might be more

illuminating than the commonly used ionic models. For example, the unique iron complex  $(^t\text{-Bu}_2\text{ap})_3\text{Fe}$  with an  $S = 0$  ground state and short Fe-ligand distances might be more simply described with a covalent model, as the ionic description requires a rather convoluted coupling scheme.<sup>43</sup> The MOS of this compound,  $-1.00(6)$ , is in line with the periodic trends of the Os and Ru compounds, and differs from the value of  $-0.84(9)$  shown by the  $S = 1$  iron compounds.

## Conclusions

Bis(iminoxolene)osmium complexes *cis*- $\beta$ -(Clip)Os(OCH<sub>2</sub>CH<sub>2</sub>O), *cis*- $\beta$ -(Clip)OsCl<sub>2</sub>, and *trans*-(Clip)Os(py)<sub>2</sub> can be prepared from the 2,2'-biphenylene-bridged bis(aminophenol) ClipH<sub>4</sub>, and tris(iminoxolene)osmium and -ruthenium complexes (MeClamp)M can be prepared from the tris(aminophenol) MeClampH<sub>6</sub>. A general electronic description of the compounds can be formulated based on emphasizing the common presence of strong, covalent metal-iminoxolene  $\pi$  bonding whose effects are modulated by the geometry of the complexes and the total number of valence electrons that are present. This approach efficiently predicts the spectroscopic and electrochemical features of the complexes without the need to invoke multiple complex magnetic coupling schemes that would be required in a more ionic picture rooted in an oxidation state description. The generality of this approach is supported by the good correlations observed between iminoxolene structural metrics and metal-ligand  $\pi$  bond order. The sensitivity of this correlation reports on the electron distribution in the polar covalent bond. The metal-iminoxolene  $\pi$  bonding thus appears to be slightly polarized towards the ligand in the case of osmium and slightly toward the metal in the case of ruthenium.

## Conflicts of Interest

There are no conflicts to declare.

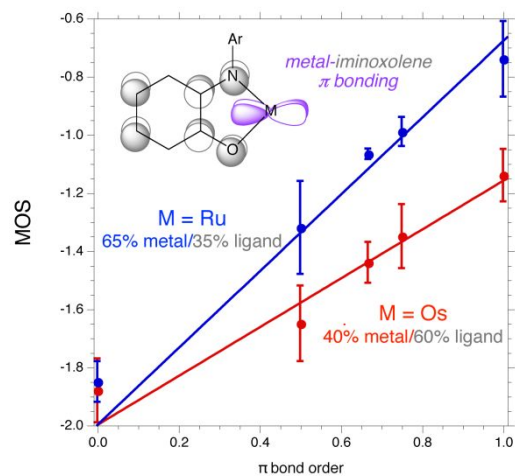
## Acknowledgments

We thank Dr. Allen G. Oliver for his assistance with the X-ray crystallography. This work was supported by the US National Science Foundation (grant CHE-1465104). J. G. gratefully acknowledges fellowship support from the US Department of Education (GAANN grant P200A1320203-14).

## Notes and references

- 1 C. G. Pierpont, *Coord. Chem. Revs.*, 2001, **216-217**, 99-125.
- 2 R. F. Munhá, R. A. Zarkesh and A. F. Heyduk, *Dalton Trans.*, 2013, **42**, 3751-3766.
- 3 X. Sun, H. Chun, K. Hildenbrand, E. Bothe, T. Weyhermüller, F. Neese and K. Wieghardt, *Inorg. Chem.*, 2002, **41**, 4295-4303.

- 4 P. Chaudhuri, C. N. Verani, E. Bill, E. Bothe, T. Weyhermüller and K. Wieghardt, *J. Am. Chem. Soc.*, 2001, **123**, 2213-2223.
- 5 T. Marshall-Roth and S. N. Brown, *Dalton Trans.*, 2015, **44**, 677-685.
- 6 A. N. Erickson and S. N. Brown, *Dalton Trans.*, 2018, **47**, 15583-15595.
- 7 S. N. Brown, *Inorg. Chem.*, 2012, 1251-1260.
- 8 C. Remenyi and M. Kaupp, *J. Am. Chem. Soc.*, 2005, **127**, 11399-11413.
- 9 A. Mandal, T. Kundu, F. Ehret, M. Bubrin, S. M. Mobin, W. Kaim and G. K. Lahiri, *Dalton Trans.*, 2014, **43**, 2473-2487.
- 10 S. Bhattacharya, P. Gupta, F. Basuli and C. G. Pierpont, *Inorg. Chem.*, 2002, **41**, 5810-5816.
- 11 D. Das, T. M. Scherer, A. Das, T. K. Mondal, S. M. Mobin, J. Fiedler, J. L. Priego, R. Jiménez-Aparicio, W. Kaim and G. K. Lahiri, *Dalton Trans.*, 2012, **41**, 11675-11683.
- 12 C. Mukherjee, T. Weyhermüller, E. Bothe and P. Chaudhuri, *Inorg. Chem.*, 2008, **47**, 11620-11632.
- 13 R. J. Collin, J. Jones and W. P. Griffith, *J. Chem. Soc., Dalton Trans.*, 1974, 1094-1097.
- 14 A. J. Godó, A. C. Bényei, B. Duff, D. A. Egan and P. Buglyó, *RSC Adv.*, 2012, **2**, 1486-1495.
- 15 N. G. Connelly and W. E. Geiger, *Chem. Rev.*, 1996, **96**, 877-910.
- 16 D. Lionetti, A. J. Medvecz, V. Ugrinova, M. Quiroz-Guzman, B. C. Noll and S. N. Brown, *Inorg. Chem.*, 2010, **49**, 4687-4697.
- 17 M. J. Frisch, G. W. Trucks, H. B. Schlegel, G. E. Scuseria, M. A. Robb, J. R. Cheeseman, G. Scalmani, V. Barone, B. Mennucci, G. A. Petersson, H. Nakatsuji, M. Caricato, X. Li, H. P. Hratchian, A. F. Izmaylov, J. Bloino, G. Zheng, J. L. Sonnenberg, M. Hada, M. Ehara, K. Toyota, R. Fukuda, J. Hasegawa, M. Ishida, T. Nakajima, Y. Honda, O. Kitao, H. Nakai, T. Vreven, J. A. Montgomery, Jr., J. E. Peralta, F. Ogliaro, M. Bearpark, J. J. Heyd, E. Brothers, K. N. Kudin, V. N. Staroverov, R. Kobayashi, J. Normand, K. Raghavachari, A. Rendell, J. C. Burant, S. S. Iyengar, J. Tomasi, M. Cossi, N. Rega, J. M. Millam, M. Klene, J. E. Knox, J. B. Cross, V. Bakken, C. Adamo, J. Jaramillo, R. Gomperts, R. E. Stratmann, O. Yazyev, A. J. Austin, R. Cammi, C. Pomelli, J. W. Ochterski, R. L. Martin, K. Morokuma, V. G. Zakrzewski, G. A. Voth, P. Salvador, J. J. Dannenberg, S. Dapprich, A. D. Daniels, O. Farkas, J. B. Foresman, J. V. Ortiz, J. Cioslowski and D. J. Fox, *Gaussian 09, Revision A.02*, Gaussian, Inc., Wallingford CT, 2009.
- 18 G. M. Sheldrick, *Acta Cryst. A*, 2008, **A64**, 112-122.
- 19 *International Tables for Crystallography*; Kluwer Academic Publishers: Dordrecht, The Netherlands, 1992, Vol C.
- 20 (a) M. R. Ringenberg, M. J. Nilges, T. B. Rauchfuss and S. R. Wilson, *Organometallics*, 2010, **29**, 1956-1965. (b) M. Bubrin, D. Schweinfurth, F. Ehret, S. Zális, H. Kvapilová, J. Fiedler, Q. Zeng, F. Hartl and W. Kaim, *Organometallics*, 2014, **33**, 4973-4985.
- 21 P. D. Knight and P. Scott, *Coord. Chem. Rev.*, 2003, **242**, 125-143.
- 22 (a) J. A. Kopeck, S. Shekar and S. N. Brown, *Inorg. Chem.*, 2012, **51**, 1239-1250. (b) S. Shekar and S. N. Brown, *Dalton Trans.*, 2014, **43**, 3601-3611.
- 23 K. M. Conner, A. L. Perugini, M. Malabute and S. N. Brown, *Inorg. Chem.*, 2018, **57**, 3272-3286.
- 24 R. Hübner, B. Sarkar, J. Fiedler, S. Zális and W. Kaim, *Eur. J. Inorg. Chem.*, 2012, 3569-3576.
- 25 N. Bag, G. K. Lahiri, P. Basu and A. Chakravorty, *J. Chem. Soc. Dalton Trans.*, 1992, 113-117.
- 26 A. K. Das, R. Hübner, B. Sarkar, J. Fiedler, S. Zális, G. K. Lahiri and W. Kaim, *Dalton Trans.*, 2012, **41**, 8913-8921.
- 27 D. Das, A. K. Das, B. Sarkar, T. K. Mondal, S. M. Modin, J. Fiedler, S. Zális, F. A. Urbanos, R. Jiménez-Aparicio, W. Kaim and G. K. Lahiri, *Inorg. Chem.*, 2009, **48**, 11853-11864.
- 28 T. Marshall-Roth, K. Yao, J. A. Parkhill and S. N. Brown, *Dalton Trans.*, 2019, **48**, 1427-1435.
- 29 (a) F. A. Cotton, J. L. Eglin, B. Hong and C. A. James, *Inorg. Chem.*, 1993, **32**, 2104-2106. (b) F. A. Cotton, J. Su, Z. S. Sun and H. Chen, *Inorg. Chem.*, 1993, **32**, 4871-4875. (c) C. E. Kriley, P. E. Fanwick and I. P. Rothwell, *J. Am. Chem. Soc.*, 1994, **116**, 5225-5232. (d) R. L. Miller, K. A. Lawler, J. L. Bennett and P. T. Wolczanski, *Inorg. Chem.*, 1996, **35**, 3242-3253. (e) B. Le Guennic, T. Floyd, B. R. Galan, J. Autschbach and J. B. Keister, *Inorg. Chem.*, 2009, **48**, 5504-5511. (f) S. Pfirrmann, C. Limberg, C. Herwig, C. Knispel, B. Braun, E. Bill and R. A. Stösser, *J. Am. Chem. Soc.*, 2010, **132**, 13684-13691. (g) J. Rittle, C. C. L. McCrory and J. C. Peters, *J. Am. Chem. Soc.*, 2014, **136**, 13853-13862. (h) T. J. Steiman and C. Uyeda, *J. Am. Chem. Soc.*, 2015, **137**, 6104-6110.
- 30 B. Chaudret, C. Cayret, H. Köster and R. Poilblanc, *J. Chem. Soc. Dalton Trans.*, 1983, 941-945.
- 31 D. D. Swanson, K. M. Conner and S. N. Brown, *Dalton Trans.*, 2017, **46**, 9049-9057.
- 32 S. M. Carter, A. Sia, M. J. Shaw and A. F. Heyduk, *J. Am. Chem. Soc.*, 2008, **130**, 5838-5839.
- 33 J. Cipressi and S. N. Brown, *Chem. Commun.*, 2014, **50**, 7956-7959.
- 34 (a) S. N. Brown, E. T. Chu, M. W. Hull and B. C. Noll, *J. Am. Chem. Soc.*, 2005, **127**, 16010-16011. (b) N. Kongprakaiwoot, M. Quiroz-Guzman, A. G. Oliver and S. N. Brown, *Chem. Sci.*, 2011, **2**, 331-336.
- 35 S. Bhattacharya and C. G. Pierpont, *Inorg. Chem.*, 1991, **30**, 1511-1516.
- 36 D. Das, T. K. Mondal, A. D. Chowdhury, F. Weisser, D. Schweinfurth, B. Sarkar, S. M. Mobin, F. A. Urbanos, R. Jimenez-Aparicio and G. K. Lahiri, *Dalton Trans.*, 2011, **40**, 8377-8390.
- 37 R. T. Sanderson, *J. Chem. Educ.*, 1988, **65**, 112-118.
- 38 D. Das, B. Sarkar, T. K. Mondal, S. M. Mobin, J. Fiedler, W. Kaim and G. K. Lahiri, *Inorg. Chem.*, 2011, **50**, 7090-7098.
- 39 A. B. P. Lever, *Coord. Chem. Rev.*, 2010, **254**, 1397-1405.
- 40 H. Chun, C. N. Verani, P. Chaudhuri, E. Bothe, E. Bill, T. Weyhermüller and K. Wieghardt, *Inorg. Chem.*, 2001, **40**, 4157-4166.
- 41 S. Mukherjee, E. Rentschler, T. Weyhermüller, K. Wieghardt and P. Chaudhuri, *Chem. Commun.*, 2003, 1828-1829.
- 42 A. Dei, D. Gatteschi, C. Sangregorio, L. Sorace and M. G. F. Vaz, *Inorg. Chem.*, 2003, **42**, 1701-1706.
- 43 S. Mukherjee, T. Weyhermüller, E. Bill, K. Wieghardt and P. Chaudhuri, *Inorg. Chem.*, 2005, **44**, 7099-7108.



Describing the  $\pi$  bonding in ruthenium and osmium iminoxolenes as highly covalent allows one to experimentally dissect the electron distribution in these compounds.